Nuclear matrix elements for the λ mechanism of $0\nu\beta\beta$ decay of ^{48}Ca in the nuclear shell-model: Closure versus nonclosure approach

Shahariar Sarkar,[1,*] Y. Iwata,[2] and P. K. Raina[1]

[1]*Indian Institute of Technology Ropar, Rupnagar, Punjab-140001, India*

[2]*Faculty of Chemistry, Materials and Bioengineering, Kansai University, Yamate-cho 3-3-35, Osaka 564-8680, Japan*

(Received 10 March 2020; revised 5 August 2020; accepted 25 August 2020; published 14 September 2020)

The λ and $m_{\beta\beta}$ mechanisms of neutrinoless double beta decay ($0\nu\beta\beta$) occur with light neutrino exchange via $W_L - W_R$ and $W_L - W_L$ mediation, respectively. In the present study, we calculate the nuclear matrix elements (NMEs) for the $m_{\beta\beta}$ and λ mechanisms of $0\nu\beta\beta$, which has origin in the left-right symmetric model with right-handed gauge boson at TeV scale. The NMEs are calculated for one of the $0\nu\beta\beta$ decaying isotope ^{48}Ca in the interacting nuclear shell-model using the GXPF1A effective interaction of pf shell. The NMEs are calculated in both closure and nonclosure approaches using four different methods: closure, running closure, running nonclosure, and mixed methods. All the NMEs are calculated incorporating the effects of the finite size of nucleons and the revisited higher-order terms such as pseudoscalar and weak magnetism terms of the nucleon currents. Inclusion of the short-range nature of nucleon-nucleon interaction in Miller-Spencer, CD-Bonn, and AV18 parametrizations is also taken care of. We have used closure energy $\langle E \rangle = 0.5$ MeV, which is near to the optimal value of closure energy that is extracted by examining the dependence of NMEs with closure energy in closure and mixed methods. The comparative dependence of the running closure and running nonclosure NMEs with the spin-parity of the allowed states of intermediate nucleus ^{48}Sc, the coupled spin-parity of the two initial decaying neutrons and the final two protons, the cutoff excitation energy of ^{48}Sc, and the cutoff number of states of ^{48}Sc are examined. The neutrino momentum and radial distribution of different types of NMEs are explored. It is found that there is a significant enhancement in M_{qGT}-type NMEs, which originates from the large momentum distribution for the inclusion of the higher-order pseudoscalar term of the nucleon currents.

DOI: 10.1103/PhysRevC.102.034317

I. INTRODUCTION

The neutrinoless double beta decay ($0\nu\beta\beta$) is an important weak nuclear process which occurs when two neutrons inside some even-even nuclei converted into two protons and two electrons. In this process neutrino comes as a virtual intermediate particle; thus it violates lepton number by two units. If this rare process is observed, then one can confirm that neutrinos are Majorana particle [1] which is favored by many theoretical particle physics models to explain the smallness of neutrino mass [1–3]. The correct value of the absolute mass scale of neutrino is still not known. Recently, the tritium β decay experiment-KATRIN have derived an upper limit of 1.1 eV (90% confidence level) on the absolute mass scale of neutrinos [4]. The $0\nu\beta\beta$ can also give some ideas about the absolute mass scale of neutrinos [5,6].

Various decay mechanisms such as the light neutrino-exchange mechanism [7,8], heavy neutrino-exchange mechanism [9], left-right symmetric mechanism [10,11], and supersymmetric particle-exchange mechanism [12,13] have been proposed for $0\nu\beta\beta$.

In the present work, we focus on the λ mechanism (W_L-W_R exchange) along with the standard $m_{\beta\beta}$ mechanism ($W_L - W_L$ exchange) of the $0\nu\beta\beta$ mediated by light neutrinos [14]. The λ mechanism originates from the left-right symmetric mechanism with right-handed gauge boson at the TeV scale [14]. The decay rate in all of these mechanisms is related to the nuclear matrix elements (NMEs) and absolute neutrino mass. These NMEs are calculated using theoretical nuclear many-body models [15] such as the quasiparticle random phase approximation (QRPA) [9], the interacting shell-model (ISM) [16–20], the interacting boson model (IBM) [21,22], the generator coordinate method (GCM) [23], the energy density functional (EDF) theory [23,24], and the projected Hartree-Fock Bogolibov model (PHFB) [25]. Recently, *ab initio* calculations of NMEs for $0\nu\beta\beta$ of lower mass nuclei ($A = 6$–12) have been also performed using the variational Monte Carlo (VMC) technique [26–28].

Earlier, in Ref. [29], the revisited formalism for the light neutrino-exchange mechanism of $0\nu\beta\beta$ is exploited to include the effects of pseudoscalar term of nucleon currents. Using the revisited formalism of Ref. [29], the NMEs for λ and $m_{\beta\beta}$ mechanisms of $0\nu\beta\beta$ are calculated using the QRPA model for several $0\nu\beta\beta$ decaying isotopes using closure approximation in Ref. [14]. In this case, the weak magnetism term of the nucleon currents is also considered for calculating the NMEs of $m_{\beta\beta}$ mechanism. Most of the NMEs relevant for λ and $m_{\beta\beta}$ mechanisms are calculated using the ISM in Ref. [30] using the closure approximation for ^{48}Ca and few other $0\nu\beta\beta$

*shahariar.sarkar@iitrpr.ac.in

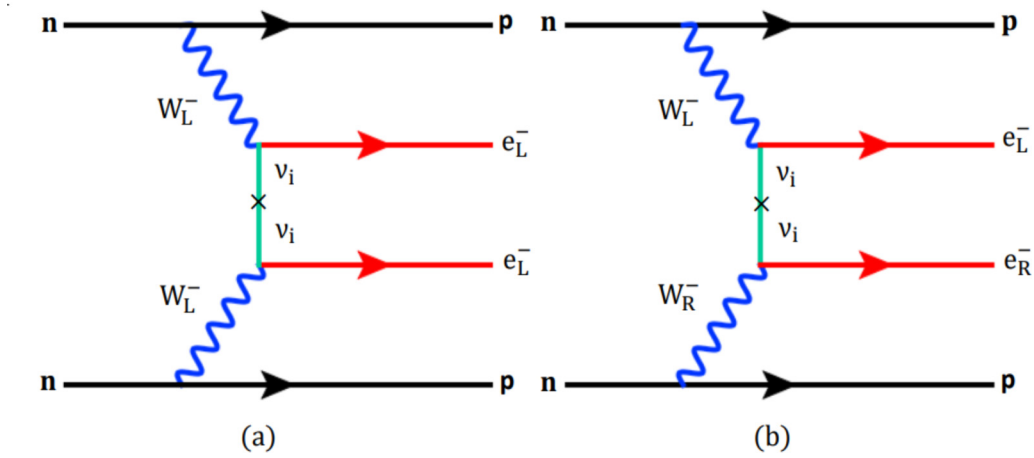

FIG. 1. The Feynman diagrams for $0\nu\beta\beta$ via (a) $W_L - W_L$ mediation ($m_{\beta\beta}$ mechanism) and (b) $W_L - W_R$ mediation (λ mechanism) with light neutrino exchange.

decaying isotopes. In this case, some of the NMEs are calculated without including the higher-order terms (pseudoscalar and weak magnetism) of the nucleon currents.

In the present study, the NMEs for the λ, and $m_{\beta\beta}$ mechanisms of $0\nu\beta\beta$ of ^{48}Ca are calculated using ISM incorporating the effects of pseudoscalar and weak magnetism terms of nucleon currents. Earlier, the nonclosure approach is applied in ISM for calculating NMEs only for the $m_{\beta\beta}$ mechanism of $0\nu\beta\beta$ of ^{48}Ca in Ref. [18]. In this work, we use both closure and nonclosure approaches to calculate the NMEs for both the λ and $m_{\beta\beta}$ mechanisms of $0\nu\beta\beta$ of ^{48}Ca.

The $0\nu\beta\beta$ process for ^{48}Ca is written as

$$^{48}\mathrm{Ca} \rightarrow ^{48}\mathrm{Ti} + e^- + e^-. \tag{1}$$

In our calculation, the short-range nature of the nucleon-nucleon interaction is also taken care of in Miller-Spencer, CD-Bonn, and AV18-type short-range correlation (SRC) parametrization [8,17]. The NMEs are calculated using the widely used pf-shell interaction GXPF1A. Using both the closure and nonclosure approaches, the NMEs are calculated in four different methods: closure, running closure, running nonclosure, and mixed methods [18].

This paper is organized as follows. In Sec. II, the expression for decay rate and the theoretical formalism to calculate NMEs for the λ and $m_{\beta\beta}$ mechanisms of $0\nu\beta\beta$ are presented. The descriptions of different methods of NME calculation based on closure and nonclosure approaches are given in Sec. III. The results and discussion are presented in Sec. IV. The summary of the work is given in Sec. V.

II. DECAY RATE FOR λ MECHANISM OF $0\nu\beta\beta$

The Feynman diagrams for the light neutrino-exchange $m_{\beta\beta}$ and λ mechanisms are shown in Fig. 1. The decay rate for $0\nu\beta\beta$, when both the mechanisms coexist, can be written as [14,29]

$$\left[T_{1/2}^{0\nu}\right]^{-1} = \eta_\nu^2 C_{mm} + \eta_\lambda^2 C_{\lambda\lambda} + \eta_\nu \eta_\lambda \cos\psi C_{m\lambda}, \tag{2}$$

where η_ν is effective lepton number violating parameters for $W_L - W_L$ exchange and η_λ is effective lepton number violating parameters for $W_L - W_R$ exchange, which are given by [14]

$$\eta_\nu = \frac{m_{\beta\beta}}{m_e}, \quad \eta_\lambda = \lambda \left| \sum_{j=1}^{3} m_j U_{ej} T_{ej}^* \right|, \tag{3}$$

$$\psi = \arg\left[\left(\sum_{j=1}^{3} m_j U_{ej}^2 \right) \left(\sum_{j=1}^{3} U_{ej} T_{ej}^* \right) \right]. \tag{4}$$

Here $m_{\beta\beta}$ is the effective Majorana neutrino mass defined by the neutrino mass eigenvalues m_j and the neutrino mixing matrix elements U_{ej} [17]:

$$\langle m_{\beta\beta} \rangle = \left| \sum_j m_j U_{ej}^2 \right|, \tag{5}$$

where U and T are the 3×3 block matrices in flavor space, which constitute a generalization of the Pontecorvo-Maki-Nakagawa-Sakata matrix, namely the 6×6 unitary neutrino mixing matrix [14,29]. The coefficients C_I ($I = mm$, $m\lambda$, and $\lambda\lambda$) are linear combinations of products of nuclear matrix elements and phase-space factors [14],

$$C_{mm} = g_A^4 M_\nu^2 G_{01}, \tag{6}$$

$$C_{m\lambda} = -g_A^4 M_\nu (M_{2-} G_{03} - M_{1+} G_{04}), \tag{7}$$

$$C_{\lambda\lambda} = g_A^4 \left(M_{2-}^2 G_{02} + \tfrac{1}{9} M_{1+}^2 G_{011} - \tfrac{2}{9} M_{1+} M_{2-} G_{010} \right). \tag{8}$$

Calculated values of phase-space factors G_{0i} ($i = 1$, 2, 3, 4, 10, and 11) for different $0\nu\beta\beta$ decaying nuclei are given in Ref. [29]. Matrix elements required in the expression of C_I are [14]

$$M_\nu = M_{GT} - \frac{M_F}{g_A^2} + M_T, \tag{9}$$

$$M_{\nu\omega} = M_{\omega GT} - \frac{M_{\omega F}}{g_A^2} + M_{\omega T}, \tag{10}$$

$$M_{1+} = M_{qGT} + 3\frac{M_{qF}}{g_A^2} - 6M_{qT}, \tag{11}$$

$$M_{2-} = M_{\nu\omega} - \frac{1}{9} M_{1+}. \tag{12}$$

The $(M_{GT,\omega GT,qGT})$, $(M_{F,\omega F,qF})$, and $(M_{T,\omega T,qT})$ matrix elements of the scalar two-body transition operator $\mathcal{O}^{\alpha}_{12}$ of $0\nu\beta\beta$ can be expressed as [19]

$$M_{\alpha} = \langle f|\tau_{-1}\tau_{-2}\mathcal{O}^{\alpha}_{12}|i\rangle, \tag{13}$$

where $|i\rangle$ and $|f\rangle$ are the initial and the final 0^{+} ground state for $0\nu\beta\beta$ decay, respectively, $\alpha = (GT, F, T, \nu, \omega GT, \omega F, \omega T, \nu\omega, qGT, qF, qT, 1+, 2-)$, and τ_{-} is the isospin annihilation operator. The scalar two-particle transition operators $\mathcal{O}^{\alpha}_{12}$ of $0\nu\beta\beta$ containing spin and radial neutrino potential operators can be written as

$$\begin{aligned}
\mathcal{O}^{GT,\omega GT,qGT}_{12} &= \tau_{1-}\tau_{2-}(\sigma_{\mathbf{1}}.\sigma_{\mathbf{2}})H_{GT,\omega GT,qGT}(r, E_k),\\
\mathcal{O}^{F,\omega F,qF}_{12} &= \tau_{1-}\tau_{2-}H_{F,\omega F,qF}(r, E_k),\\
\mathcal{O}^{T,\omega T,qT}_{12} &= \tau_{1-}\tau_{2-}S_{12}H_{T,\omega T,qT}(r, E_k),
\end{aligned} \tag{14}$$

where $S_{12} = 3(\sigma_{\mathbf{1}}.\hat{\mathbf{r}})(\sigma_{\mathbf{2}}.\hat{\mathbf{r}}) - (\sigma_{\mathbf{1}}.\sigma_{\mathbf{2}})$, $\mathbf{r} = \mathbf{r_1} - \mathbf{r_2}$, and $r = |\mathbf{r}|$ is internucleon distance of the decaying nucleons.

The neutrino potential for λ mechanism of $0\nu\beta\beta$ are given as an integral over the Majorana neutrino momentum q [18]:

$$H_{\alpha}(r, E_k) = \frac{2R}{\pi}\int_0^{\infty}\frac{f_{\alpha}(q, r)qdq}{q + E_k - (E_i + E_f)/2}, \tag{15}$$

where R is the radius of the parent nucleus, E_k is the energy of the intermediate states, E_i is the energy of the initial state, E_f is the energy of the final state, and the $f_{\alpha}(q, r)$ factor contains the form factors that incorporates the effects of finite nucleon size (FNS) and higher-order currents (HOC) of nucleons [8]. The $f_{\alpha}(q, r)$ factor can be written in terms of radial dependence, spherical Bessel function $j_p(qr)(p = 0, 1, 2, \text{and } 3)$, and FNS + HOC coupling form factors as [14]

$$\begin{aligned}
f_{GT}(q, r) = \frac{j_0(qr)}{g_A^2}\Bigg\{g_A^2(q^2) - \frac{g_A(q^2)g_P(q^2)}{m_N}\frac{q^2}{3}\\
+\frac{g_P^2(q^2)}{4m_N^2}\frac{q^4}{3} + \left[2\frac{g_M^2(q^2)}{4m_N^2}\frac{q^2}{3}\right]\Bigg\},
\end{aligned} \tag{16}$$

$$f_F(q, r) = g_V^2(q^2)j_0(qr), \tag{17}$$

$$\begin{aligned}
f_T(q, r) = \frac{j_2(qr)}{g_A^2}\Bigg[\frac{g_A(q^2)g_P(q^2)}{m_N}\frac{q^2}{3} - \frac{g_P^2(q^2)}{4m_N^2}\frac{q^4}{3}\\
+\frac{g_M^2(q^2)}{4m_N^2}\frac{q^2}{3}\Bigg],
\end{aligned} \tag{18}$$

$$f_{\omega GT}(q, r) = \frac{q}{[q + E_k - (E_i + E_f)/2]}f_{GT}(q, r), \tag{19}$$

$$f_{\omega F}(q, r) = \frac{q}{[q + E_k - (E_i + E_f)/2]}f_{F}(q, r), \tag{20}$$

$$f_{\omega T}(q, r) = \frac{q}{[q + E_k - (E_i + E_f)/2]}f_{T}(q, r), \tag{21}$$

$$\begin{aligned}
f_{qGT}(q, r) = \Bigg[\frac{g_A^2(q^2)}{g_A^2}q + 3\frac{g_P^2(q^2)}{g_A^2}\frac{q^5}{4m_N^2}\\
+\frac{g_A(q^2)g_P(q^2)}{g_A^2}\frac{q^3}{m_N}\Bigg]rj_1(q, r),
\end{aligned} \tag{22}$$

$$f_{qF}(q, r) = rg_V^2(q^2)j_1(qr)q, \tag{23}$$

$$\begin{aligned}
f_{qT}(q, r) = \frac{r}{3}\Bigg(\left[\frac{g_A^2(q^2)}{g_A^2}q - \frac{g_P(q^2)g_A(q^2)}{2g_A^2}\frac{q^3}{m_N}\right]j_1(qr)\\
-\left\{9\frac{g_P^2(q^2)}{2g_A^2}\frac{q^5}{20m_N^2}[2j_1(qr)/3 - j_3(qr)]\right\}\Bigg),
\end{aligned} \tag{24}$$

where one can write in dipole approximation [8]

$$g_V(q^2) = \frac{g_V}{\left(1 + \frac{q^2}{M_V^2}\right)^2}, \tag{25}$$

$$g_A(q^2) = \frac{g_A}{\left(1 + \frac{q^2}{M_A^2}\right)^2}, \tag{26}$$

$$g_M(q^2) = (\mu_p - \mu_n)g_V(q^2), \tag{27}$$

$$g_P(q^2) = \frac{2m_p g_A(q^2)}{(q^2 + m_{\pi}^2)}\left(1 - \frac{m_{\pi}^2}{M_A^2}\right), \tag{28}$$

where $\mu_p - \mu_n = 4.7$, $M_V = 850\,\text{MeV}$, and $M_A = 1086\,\text{MeV}$ m_p and m_{π} are the mass of protons and pions [18]. In the present calculation, vector constant $g_V = 1.0$ and bare axial-vector constant $g_A = 1.27$ [31] is used. Both the pseudoscalar and weak magnetism terms of the nucleon currents are included in $f_{GT,T,\omega GT,\omega T}(q, r)$ factors, whereas pseudoscalar term is included in $f_{qGT,qT}(q, r)$ factors [14].

The short-range nature of the two-nucleon interaction is taken care by multiplying relative harmonic oscillator wave function ψ_{nl} in the radial integral $\langle n', l'|H_{\alpha}(r)|n, l\rangle$ with a correlation function $f(r)$ [17],

$$\psi_{nl}(r) \longrightarrow [1 + f(r)]\psi_{nl}(r), \tag{29}$$

where $f(r)$ can be parametrized as [32]

$$f(r) = -ce^{-ar^2}(1 - br^2). \tag{30}$$

The parameters a, b, and c for Miller-Spencer, CD-Bonn, and AV18-type SRC parametrizations are given in Ref. [17].

III. CLOSURE, NONCLOSURE, AND MIXED METHODS

A. Closure approach

In the closure approach, one replaces the term $[E_k - (E_i + E_f)/2]$ in Eq. (15) by an average closure energy $\langle E\rangle$:

$$[E_k - (E_i + E_f)/2] \to \langle E\rangle.$$

In the closure approach, the neutrino potential of Eq. (15) becomes

$$H_{\alpha}(r) = \frac{2R}{\pi}\int_0^{\infty}\frac{f_{\alpha}(q, r)qdq}{q + \langle E\rangle}, \tag{31}$$

and the transition operators of $0\nu\beta\beta$ of Eq. (14) can be rewritten as

$$\begin{aligned}
O^{GT,\omega GT,qGT}_{12} &= \tau_{1-}\tau_{2-}(\sigma_{\mathbf{1}}.\sigma_{\mathbf{2}})H_{GT,\omega GT,qGT}(r),\\
O^{F,\omega F,qF}_{12} &= \tau_{1-}\tau_{2-}H_{F,\omega F,qF}(r),\\
O^{T,\omega T,qT}_{12} &= \tau_{1-}\tau_{2-}S_{12}H_{T,\omega T,qT}(r).
\end{aligned} \tag{32}$$

The closure approach has a significant advantage over the nonclosure approach because it eliminates the complexity

of calculating NMEs in terms of excitation energy of a large number of the intermediate states, which can be computationally challenging for heavy nuclear systems. This approximation is also very good as the values of q that dominate the matrix elements are of the order of $\approx$ 100–200 MeV, whereas the relevant excitation energies of the intermediate states are about 10 MeV [18]. One important part of closure approximation is to use a suitable value of average closure energy $\langle E\rangle$ that will take care of the combined effects of a large number of intermediate states. In the present work, we have used closure energy $\langle E\rangle = 0.5$ MeV [17,18].

B. Nonclosure approach

In the nonclosure approach, one calculates the neutrino potential of Eq. (15) explicitly in terms of energy E_k of a large number of virtual intermediate states $|k\rangle$ [for our case (^{48}Sc)]. For our nonclosure calculations, we have used [18]

$$E_k - (E_i + E_f)/2 \rightarrow 1.9\ \text{MeV} + E_k^*, \tag{33}$$

where E_k^* is the excitation energy of the intermediate states $|k\rangle$.

Descriptions of four different methods, closure, running closure, running nonclosure, and mixed methods, to calculate NMEs of $0\nu\beta\beta$ based on closure and nonclosure approaches are given below.

C. Closure method

In the closure method, the NMEs are calculated using the transition operator of Eq. (32) for the λ mechanism of $0\nu\beta\beta$ and the neutrino potential for the closure approximation defined in Eq. (31). In this method, NMEs defined in Eq. (13) can be written as the sum of the products of two-nucleon transfer amplitudes (TNAs) and antisymmetric nonreduced two-body matrix elements $\langle k_1', k_2', JT|\tau_{-1}\tau_{-2}O_{12}^{\alpha}|k_1, k_2, JT\rangle_A$ as [19]

$$\begin{aligned}\mathcal{M}_\alpha = &\sum_{m,J,k_1'\leqslant k_2',k_1\leqslant k_2} \text{TNA}(f, m, k_1', k_2', J_m)\\ &\text{TNA}(i, m, k_1, k_2, J_m)\\ &\times\langle k_1', k_2' : JT|\tau_{-1}\tau_{-2}O_{12}^{\alpha}|k_1, k_2 : JT\rangle_A,\end{aligned} \tag{34}$$

where k denotes the set of spherical quantum numbers $(n; l; j)$ and A denotes that the two-body matrix elements are obtained using an antisymmetric two-nucleon wave function. In our study, $|i\rangle$ is 0^+ ground state of the parent nucleus ^{48}Ca, $|m\rangle$ is the large number of states of intermediate nucleus (^{46}Ca) with allowed spin-parity (J^π) (for TNA calculation), $|f\rangle$ is the 0^+ ground state of the granddaughter nucleus ^{48}Ti, and k has the spherical quantum numbers for $0f_{7/2}$, $0f_{5/2}$, $1p_{3/2}$, and $1p_{1/2}$ orbitals. Complete expression of antisymmetric nonreduced two-body matrix elements (TBMEs) is given in Refs. [17,31].

TNA is calculated with a large set of intermediate states $|m\rangle$ of the $(n-2)$ nucleons system (^{46}Ca in the present study), where n is the number of nucleons for the parent nucleus. TNA is given by [19]

$$\text{TNA}(f, m, k_1', k_2', J_m) = \frac{\langle f||A^+(k_1', k_2', J_m)||m\rangle}{\sqrt{2J_0+1}}. \tag{35}$$

Here

$$A^+(k_1', k_2', J_m) = \frac{[a^+(k_1')\otimes a^+(k_2')]_M^{J_m}}{\sqrt{1+\delta_{k_1'k_2'}}} \tag{36}$$

is the two particle creation operator of rank J, J_m is the spin of the allowed states of ^{46}Ca, J_0 is spin of $|i\rangle$ and $|f\rangle$. In Eq. (34) $J_m = J$ when $J_0 = 0$ [19]. The TNA is normalized such that

$$\text{TNA}^2 = n_p(n_p-1)/2 \tag{37}$$

for the removal of two protons and

$$\text{TNA}^2 = n_n(n_n-1)/2 \tag{38}$$

for the removal of two neutrons, where $n_{p(n)}$ are the total number of protons (neutrons) in the model-space [19].

D. Running closure method

In the running closure method, one uses the same $0\nu\beta\beta$ transition operator and neutrino potential as a closure method. However, in this method, one gets the true virtual intermediate nucleus after one neutron from parent nucleus decay into one proton. In the present study, ^{48}Sc is the true virtual intermediate nucleus. For convenience we can write the partial nuclear matrix elements of running closure method in proton-neutron (pn) formalism as function of the spin-parity of the states of the intermediate nucleus (J_k^π), the coupled-spin of two decaying protons or the two final created protons (J^π), and the excitation energy of the states of the virtual intermediate nucleus (E_k^*) as sum over products of one body transition density (OBTD) and non-anti-symmetric reduced two-body matrix elements $\langle k_1', k_2' : J||\tau_{-1}\tau_{-2}O_{12}^{\alpha}||k_1, k_2 : J\rangle$ as [18,33]:

$$\begin{aligned}\mathcal{M}_\alpha(J_k, J, E_k^*) = &\sum_{k_1'k_2'k_1k_2}\sqrt{(2J_k+1)(2J_k+1)(2J+1)}\\ &\times(-1)^{j_{k1}+j_{k2}+J}\begin{Bmatrix} j_{k1'} & j_{k1} & J_k\\ j_{k2} & j_{k2'} & J\end{Bmatrix}\\ &\times\text{OBTD}(k, f, k_2', k_2, J_k)\\ &\times\text{OBTD}(k, i, k_1', k_1, J_k)\langle k_1', k_2' : J|\\ &\times\left|\tau_{-1}\tau_{-2}O_{12}^{\alpha}\right||k_1, k_2 : J\rangle.\end{aligned} \tag{39}$$

Here k_1 represents set of spherical quantum numbers (n_1, l_1, j_1) for an orbital. Now the final NME in running closure method can be written as

$$\mathcal{M}_\alpha(E_c) = \sum_{J_k,J,E_k^*\leqslant E_c}\mathcal{M}_\alpha^{0\nu}(J_k, J, E_k^*), \tag{40}$$

where E_k^* of each allowed J_k^π of intermediate nucleus can run up to cutoff excitation energy E_c in the summation. Considering states whose excitation energy E_k^* goes up to E_c gives almost constant NMEs when E_c is large enough. OBTD in proton-neutron formalism can be written as [18]

$$\text{OBTD}(k, i, k_1', k_1, \mathcal{J}) = \frac{\langle k||\left[a_{k_1'}^+\otimes\tilde{a}_{k_1}\right]_{\mathcal{J}}||i\rangle}{\sqrt{2\mathcal{J}+1}}, \tag{41}$$

where $a_{k_1'}^+$ and $\tilde{a}_{k_1}$ are the one particle creation and annihilation operator, respectively. In the present study $|k\rangle$ is the large

number of virtual intermediate states of ^{48}Sc for different allowed J_k^π.

E. Running nonclosure method

In the running nonclosure method, NMEs are calculated with the nonclosure $0\nu\beta\beta$ transition operators given in Eq. (14). Nonclosure neutrino potential defined in Eq. (15) are calculated explicitly in terms of excitation energy of large number allowed states of intermediate nucleus (^{48}Sc). Partial NMEs for running nonclosure in proton-neutron formalism can be defined as [18,33]

$$\begin{aligned} M_\alpha(J_k, J, E_k^*) = & \sum_{k_1' k_2' k_1 k_2} \sqrt{(2J_k+1)(2J_k+1)(2J+1)} \\ & \times (-1)^{j_{k1}+j_{k2}+J} \begin{Bmatrix} j_{k1'} & j_{k1} & J_k \\ j_{k2} & j_{k2'} & J \end{Bmatrix} \\ & \times \mathrm{OBTD}(k, f, k_2', k_2, J_k) \\ & \times \mathrm{OBTD}(k, i, k_1', k_1, J_k) \langle k_1', k_2' : J| \\ & \times \left|\tau_{-1}\tau_{-2}\mathcal{O}_{12}^\alpha\right| |k_1, k_2 : J\rangle, \end{aligned} \tag{42}$$

where the above Eq. (42) is similar to Eq. (39), except the transition operator $\mathcal{O}_{12}^{0\nu}$, which has explicit E_k^* dependence. The final NME in the running nonclosure method is given by [18]

$$M_\alpha(E_c) = \sum_{J_k, J, E_k^* \leqslant E_c} M_\alpha(J_k, J, E_k^*). \tag{43}$$

The complete expression of non-anti-symmetric reduced TBMEs for the running nonclosure and running closure methods is given in Ref. [18].

F. Mixed method

The mixed method is the superposition of the running nonclosure, running closure, and closure methods. NMEs in the mixed method are written as [18]

$$\bar{M}_\alpha(E_c) = M_\alpha(E_c) - \mathcal{M}_\alpha(E_c) + \mathcal{M}_\alpha. \tag{44}$$

In this context, we want to mention that in Ref. [18] NMEs in the closure method part of the above Eq. (44) are calculated in the pure closure method [17]. The shell model code NushellX@MSU [34], which is used in our calculation, does not give a direct option to calculate required two-body transition density (TBTD) [17] for the pure closure method. Hence, we calculate NMEs in the closure method using Eq. (34) in terms of TNA, which is first introduced in Ref. [19] and also used in Ref. [31]. One can expect a negligible difference in NMEs with the closure and pure closure methods when TNA satisfies Eqs. (37) and (38).

The mixed method has very good convergence property [18]. Thus, this method is particularly useful for calculating NMEs for higher-mass-region isotopes. Because of high convergence, NMEs calculated with few states of the intermediate nucleus can give almost constant NMEs.

IV. RESULTS AND DISCUSSION

All necessary OBTD and TNA are calculated using the shell-model code NushellX@MSU [34]. For calculating OBTD, first 150 states are considered for each allowed spin-parity (J_k^π) of virtual intermediate state ^{48}Sc for $0\nu\beta\beta$ of ^{48}Ca. TNA are calculated with ^{46}Ca as an intermediate state for $0\nu\beta\beta$ of ^{48}Ca. The first 100 states are considered for each allowed spin-parity of ^{46}Ca (J_m^π). Antisymmetric nonreduced two-body matrix elements for the closure method and reduced non-anti-symmetric two-body matrix elements for the running closure and running nonclosure methods are calculated by a program written by us.

A. The optimal closure energy ($\langle E \rangle$) and the dependence of NME on $\langle E \rangle$

In our calculation, we have used the closure energy $\langle E \rangle = 0.5$ MeV, which is near the optimal value of closure energy. At optimal $\langle E \rangle$, NMEs in the closure and mixed methods have the same value, which is near the NME in the running nonclosure method. To find the optimal $\langle E \rangle$, we have examined the dependence of different types of total NMEs, calculated in the closure and mixed methods, with $\langle E \rangle$ for AV18 SRC parametrization. The variations are shown in Fig. 2.

At optimal $\langle E \rangle$, the NME in the mixed method (solid red line) crosses the NME in the closure method (dotted black line), which is marked with a vertical dashed blue line. The optimal values of $\langle E \rangle$ are found to be 0.20, 0.65, 0.30, and 0.67 MeV for M_ν-, $M_{\nu\omega}$-, M_{1+}-, and M_{2-}-type NMEs, respectively. The optimal $\langle E \rangle$ for M_ν-type NMEs was also found to be around 0.20 MeV in Fig. 2 of Ref. [31] for AV18-type SRC parametrization with GXPF1A interaction and in Fig. 3 of Ref. [35] for GXPF1A interaction.

Also, in Refs. [19,20,31], $\langle E \rangle = 0.5$ MeV is used as the optimal value for M_ν-type NMEs for ^{48}Ca, which is very close to the optimal value found by examining the dependence of NME in closure and mixed methods with $\langle E \rangle$.

At the optimal $\langle E \rangle$, NMEs calculated in the closure, running closure, and mixed methods are given in Table I for AV18-type SRC parametrization with GXPF1A interaction. Also, NMEs are presented for $\langle E \rangle = 0.5$ MeV, which is close to the optimal value and used in many earlier works. We found that at optimal $\langle E \rangle$, the NMEs in the closure and mixed methods have the same value. When using $\langle E \rangle = 0.5$ MeV instead of the optimal value, we found that there is less than a 1% change of NME. Thus, $\langle E \rangle = 0.5$ is a suitable closure energy and is used in all our calculations of NME for $0\nu\beta\beta$ of ^{48}Ca. It is useful to coherently compare different types of NMEs at single closure energy without affecting the accuracy of NMEs. The NMEs in the running closure methods at optimal $\langle E \rangle$ are not exactly the same as the NMEs in the closure and mixed methods, but they are near those NMEs. We have also shown the variation of different types of total NMEs in the running closure and mixed methods with closure energy $\langle E \rangle$ in Fig. 3. The NMEs shown here are calculated with total GXPF1A interaction for AV18-type SRC parametrization. It is observed that for changing $\langle E \rangle = 0$ to 10 MeV, there are about 11% decrements of M_ν-type NMEs in the running closure method.

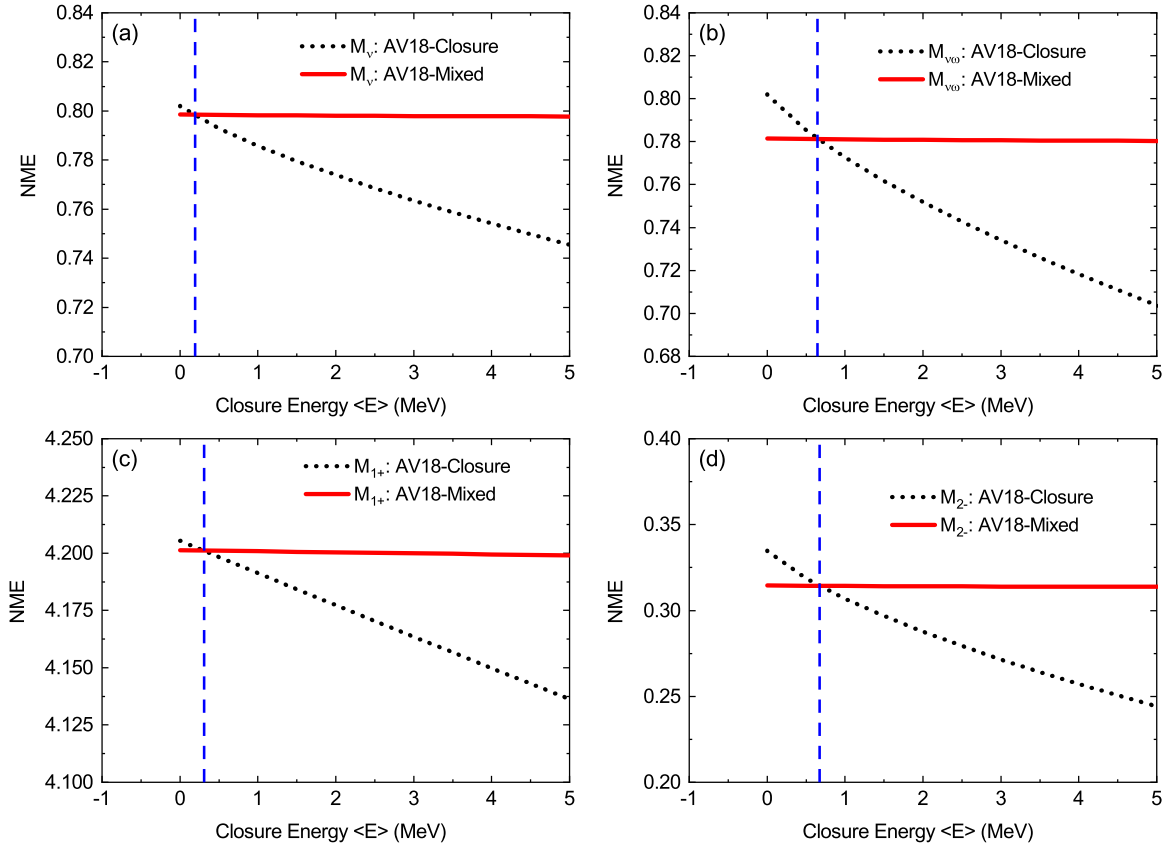

FIG. 2. Dependence of (a) M_ν-, (b) $M_{\nu\omega}$-, (c) M_{1+}-, and (d) M_{2-}-type NMEs with closure energy $\langle E\rangle$, calculated with closure and mixed methods using the GXPF1A interaction for AV18 SRC parametrization. At optimal $\langle E\rangle$, the NME in the mixed method (solid red line) crosses the NME in the closure method (dotted black line), which is marked with vertical dashed blue line.

In this case, $M_{\nu\omega}$-type NMEs decrease by about 19%, and M_{1+}-type NMEs decrease by about 3% in the running closure method. In all these cases, we found negligible changes in NMEs in the mixed method. A similar pattern of variation of NMEs with $\langle E\rangle$ is found with other SRC parametrizations.

B. Comparison of NME in different methods

Calculated NMEs M_F, M_{GT}, M_T, and M_ν are given in Table II. The $M_{\omega F}$-, $M_{\omega GT}$-, $M_{\omega T}$-, and $M_{\nu\omega}$-type NMEs are presented in Table III and the M_{qF}-, M_{qGT}-, M_{qT}-, $M_{\nu q}$-, M_{1+}-, and M_{2-}-type NMEs are given in Table IV.

From Table II, it is found for different SRC parametrizations that the $M_{F,GT,0\nu}$-type NMEs calculated in the running closure method are near the NMEs in the closure method. In this case, NMEs in the running nonclosure method are up to 2% larger in magnitude than the corresponding NMEs in the running closure method. The NMEs in the mixed method are also close to the NMEs in the running nonclosure method. The M_T-type NMEs calculated in the running closure method

TABLE I. The M_ν, $M_{\nu\omega}$, M_{1+}, and M_{2-} NMEs, calculated with the GXPF1A interaction in the closure, running closure, and mixed methods for AV18 SRC parametrization with the optimal value of $\langle E\rangle$. The results for $\langle E\rangle = 0.5$ MeV, which is close to the optimal value and used in earlier works [19,20,31], are also given.

NME	$\langle E\rangle$ (MeV)	Running closure	Closure	Mixed
M_ν	0.20	0.797	0.798	0.798
M_ν	0.50	0.792	0.793	0.799
$M_{\nu\omega}$	0.65	0.781	0.781	0.781
$M_{\nu\omega}$	0.50	0.785	0.785	0.781
M_{1+}	0.30	4.158	4.201	4.201
M_{1+}	0.50	4.157	4.196	4.200
M_{2-}	0.67	0.319	0.314	0.314
M_{2-}	0.50	0.323	0.319	0.314

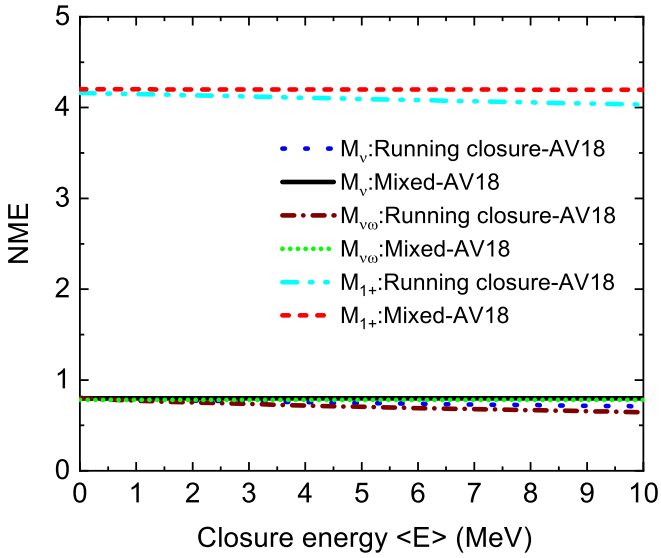

FIG. 3. Dependence of the total NMEs for $0\nu\beta\beta$ (λ and $m_{\beta\beta}$ mechanisms) of ^{48}Ca with closure energy $\langle E\rangle$, calculated with total GXPF1A interaction for AV18 SRC parmaetrization in the running closure and mixed methods.

are about 4% smaller in magnitude than the corresponding NMEs in the closure method. In this case, the NMEs in the running nonclosure method are similar to the corresponding NMEs in the running closure method, and the NMEs in the mixed method are about 4% larger than the corresponding NMEs in the running nonclosure method.

The very small difference of NME in the closure and nonclosure methods are shown for using near optimal closure energy $\langle E\rangle = 0.5$ MeV. If one uses the old standard closure energy $\langle E\rangle = 7.72$ MeV, which is suggested by QRPA calculations [5], then one would expect larger difference of 10% or more between closure and nonclosure NME [18]. But using $\langle E\rangle = 0.5$ MeV is more relevant as suggested in earlier works [19,20,31] and in Fig. 2 of the present study.

From Table III, it is found for different SRC parametrizations that the $M_{\omega F}$-type NMEs calculated in the running nonclosure method are about 2–4% larger in magnitude than the corresponding NMEs in the running closure method.

The $M_{\omega GT}$-type NMEs calculated in the running nonclosure method are about 3% larger than the corresponding NMEs in the running closure method for Miller-Spencer-type SRCs. For other SRC parametrizations, NMEs are similar. The $M_{\omega T}$-type NMEs calculated in the running closure method are up to 4% smaller in magnitude than the NMEs in the closure method. In this case, the NMEs in running nonclosure are similar to the corresponding NMEs in the running closure method, and the NMEs in the mixed methods are up to 4% larger than the corresponding NMEs in the running nonclosure method for different SRC parametrization. It is found for different SRC parametrizations that there are very small differences of the $M_{\nu\omega}$-type NMEs calculated in the running closure and closure methods, which leads to similar NMEs in the running nonclosure and mixed methods. In this case, NMEs in the running nonclosure method are about 2% larger than the corresponding NMEs in the running closure method for Miller-Spencer-type SRC parametrization. Most of the enhancements come through $M_{\omega GT}$-type NMEs.

From Table IV, it is found for different SRC parametrization that the M_{qF}-type NMEs calculated in running nonclosure method are up to 2% smaller in magnitude than the corresponding NMEs in running closure method. The M_{qGT}-type NMEs calculated in the running nonclosure method are up to 2% larger than the corresponding NMEs in the running closure method for CD-Bonn-type SRC parametrization. The M_{qT}-type NMEs calculated in the running closure method are about 5% smaller in magnitude

TABLE II. Nuclear matrix elements M_F, M_GT, M_T, and M_ν for $0\nu\beta\beta$ of ^{48}Ca, calculated with the GXPF1A interaction in the closure, running closure, running nonclosure, and mixed methods for different SRC parametrizations. $\langle E\rangle = 0.5$ MeV is used for the closure and running closure methods.

NME	SRC	Closure	Running closure	Running nonclosure	Mixed
M_F	None	−0.215	−0.214	−0.210	−0.211
M_F	Miller-Spencer	−0.144	−0.144	−0.143	−0.143
M_F	CD-Bonn	−0.232	−0.231	−0.226	−0.227
M_F	AV18	−0.213	−0.212	−0.207	−0.208
M_{GT}	None	0.774	0.771	0.779	0.782
M_{GT}	Miller-Spencer	0.540	0.538	0.553	0.555
M_{GT}	CD-Bonn	0.806	0.804	0.810	0.812
M_{GT}	AV18	0.740	0.737	0.745	0.748
M_T	None	−0.077	−0.074	−0.074	−0.077
M_T	Miller-Spencer	−0.078	−0.075	−0.075	−0.078
M_T	CD-Bonn	−0.079	−0.076	−0.076	−0.079
M_T	AV18	−0.079	−0.076	−0.076	−0.079
M_ν	None	0.830	0.830	0.836	0.836
M_ν	Miller-Spencer	0.552	0.552	0.566	0.566
M_ν	CD-Bonn	0.872	0.871	0.874	0.875
M_ν	AV18	0.793	0.792	0.798	0.799

TABLE III. Nuclear matrix elements $M_{\omega F}$, $M_{\omega GT}$, $M_{\omega T}$, and $M_{\nu\omega}$ for $0\nu\beta\beta$ of ^{48}Ca calculated with the GXPF1A interaction in the closure, running closure, running nonclosure, and mixed methods for different SRC parametrizations. $\langle E\rangle = 0.5$ MeV is used for the closure and running closure methods.

NME	SRC	Closure	Running closure	Running nonclosure	Mixed
$M_{\omega F}$	None	−0.215	−0.213	−0.206	−0.208
$M_{\omega F}$	Miller-Spencer	−0.144	−0.144	−0.141	−0.141
$M_{\omega F}$	CD-Bonn	−0.232	−0.230	−0.220	−0.222
$M_{\omega F}$	AV18	−0.212	−0.211	−0.202	−0.203
$M_{\omega GT}$	None	0.767	0.764	0.766	0.769
$M_{\omega GT}$	Miller-Spencer	0.535	0.532	0.546	0.549
$M_{\omega GT}$	CD-Bonn	0.799	0.796	0.794	0.797
$M_{\omega GT}$	AV18	0.732	0.730	0.731	0.733
$M_{\omega T}$	None	−0.077	−0.074	−0.073	−0.076
$M_{\omega T}$	Miller-Spencer	−0.078	−0.075	−0.074	−0.077
$M_{\omega T}$	CD-Bonn	−0.079	−0.076	−0.075	−0.078
$M_{\omega T}$	AV18	−0.079	−0.076	−0.075	−0.078
$M_{\nu\omega}$	None	0.823	0.823	0.821	0.821
$M_{\nu\omega}$	Miller-Spencer	0.547	0.547	0.559	0.559
$M_{\nu\omega}$	CD-Bonn	0.864	0.863	0.856	0.857
$M_{\nu\omega}$	AV18	0.785	0.785	0.781	0.781

than the corresponding NMEs in the closure method. In this case, the NMEs in the running nonclosure method are similar to the corresponding NMEs in the running closure method, and the NMEs in the mixed method are about 5% larger than the corresponding NMEs in the running nonclosure method for different SRC parametrizations. Both M_{qF}- and M_{qGT}-type have similar values in the closure and running closure methods, which lead to similar values of those NMEs in the running nonclosure and mixed methods.

The M_{1+}-type NMEs calculated in the running closure method are 1% smaller than the corresponding NMEs in the closure method for different SRC parametrization. Thus total NMEs in the running nonclosure method are about 2% larger than the corresponding NMEs in the running closure method

TABLE IV. Nuclear matrix elements M_{qF}, M_{qGT}, M_{qT}, M_{1+}, and M_{2-} for $0\nu\beta\beta$ of ^{48}Ca calculated with the GXPF1A interaction in the closure, running closure, running nonclosure, and mixed methods for different SRC parametrizations. $\langle E\rangle = 0.5$ MeV is used for the closure and running closure methods.

NME	SRC	Closure	Running closure	Running nonclosure	Mixed
M_{qF}	None	−0.099	−0.099	−0.101	−0.101
M_{qF}	Miller-Spencer	−0.078	−0.079	−0.080	−0.081
M_{qF}	CD-Bonn	−0.120	−0.120	−0.121	−0.121
M_{qF}	AV18	−0.116	−0.116	−0.117	−0.117
M_{qGT}	None	3.302	3.304	3.317	3.315
M_{qGT}	Miller-Spencer	2.733	2.734	2.751	2.750
M_{qGT}	CD-Bonn	3.620	3.623	3.709	3.706
M_{qGT}	AV18	3.488	3.491	3.502	3.499
M_{qT}	None	−0.152	−0.144	−0.143	−0.151
M_{qT}	Miller-Spencer	−0.155	−0.147	−0.146	−0.154
M_{qT}	CD-Bonn	−0.154	−0.146	−0.145	−0.153
M_{qT}	AV18	−0.154	−0.147	−0.146	−0.153
M_{1+}	None	4.030	3.984	3.987	4.033
M_{1+}	Miller-Spencer	3.518	3.469	3.478	3.524
M_{1+}	CD-Bonn	4.321	4.276	4.354	4.400
M_{1+}	AV18	4.196	4.157	4.160	4.200
M_{2-}	None	0.375	0.380	0.378	0.373
M_{2-}	Miller-Spencer	0.156	0.162	0.173	0.167
M_{2-}	CD-Bonn	0.384	0.388	0.372	0.367
M_{2-}	AV18	0.319	0.323	0.319	0.314

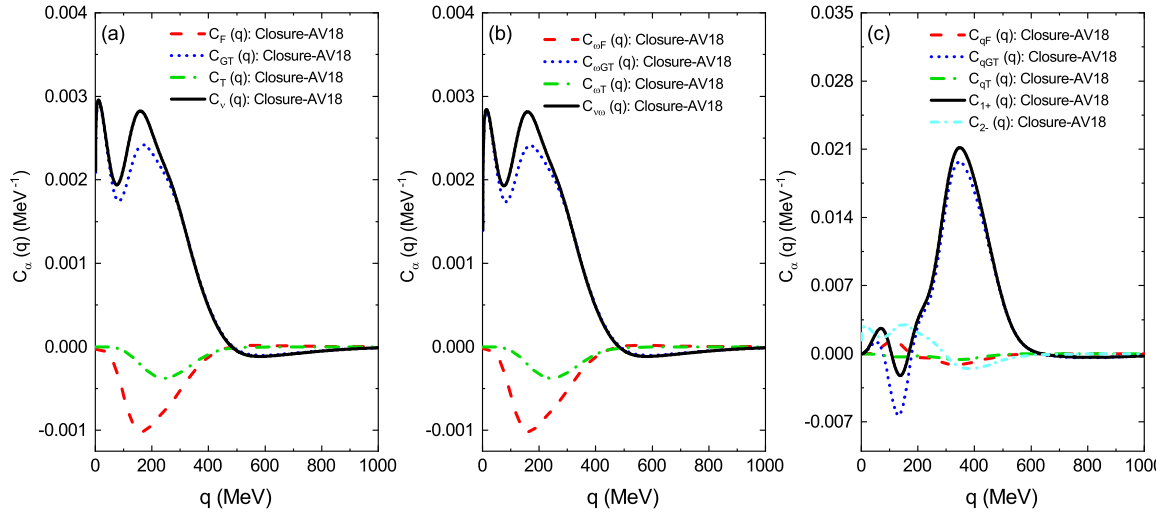

FIG. 4. Distribution of NMEs $[C_\alpha(q)]$ with neutrino momentum (q) transfer. All the NMEs are calculated with the closure method for AV18 SRC parametrization with closure energy $\langle E\rangle = 0.5$ MeV using GXPF1A interaction.

for CD-Bonn-type SRC parametrization only. In this case, the NMEs in the mixed method are about 1% larger than the corresponding NMEs in the running nonclosure method.

The M_{2-}-type NMEs calculated in the running closure method are similar to the corresponding NMEs in the closure method except for Miller-Spencer SRC parametrization. In this case, the M_{2-}-type NMEs in the running nonclosure method are about 2% smaller than the corresponding NMEs in the running closure method for CD-Bonn SRC parametrization. The NMEs in the mixed method are about 1–2% smaller than the corresponding NMEs in the running nonclosure method.

From Tables II–IV, it is found that $M_{\nu\omega}$ NMEs are about 1–2% smaller than M_ν-type NMEs in the closure, running closure, running nonclosure, and mixed methods for different SRC parametrizations. The M_{1+}-type NMEs are about 389–543%, 384–535%, 385–522%, and 390–530% larger than $M_{\nu\omega}$-type NMEs in the closure, running closure, running nonclosure, and mixed methods, respectively, for different SRC parametrizations.

This increment of M_{1+}-type of NMEs is surprisingly high, which is coming through the very large value of M_{qGT}-type NMEs as compared to M_{GT}- and $M_{\omega GT}$-type NMEs. To justify the large value of M_{qGT}-type NMEs, we have carefully checked our calculations and found that large value for M_{qGT} is coming through the new revisited expression of the nucleon currents of Ref. [14] which includes a higher-order term (pseudoscalar) of the nucleon currents. In our calculation, Eq. (22) is used to calculate M_{qGT}-type NMEs using the revisited formalism of nucleon currents of Refs. [14,29].

An old equivalent expression of Eq. (22) is also found in Ref. [30], which one can write using Eq. (A2c) and Eq. (A4b) of Ref. [30] as

$$f_{qGT}(q,r) = \frac{1}{\left(1+\frac{q^2}{\Lambda_A^2}\right)^4} qr j_1(qr). \tag{45}$$

Using Eq. (45), which does not include the higher-order terms of nucleon currents, the M_{qGT}-type NME for ^{48}Ca is reported to be 0.709 in Table XVI of Ref. [30] for CD-Bonn-type SRC parametrization with closure energy $\langle E\rangle = 0.5$ MeV. We have also performed the same calculation for M_{qGT}-type NMEs in the closure method for CD-Bonn SRC parametrization with $\langle E\rangle = 0.5$ MeV by using old factor of Eq. (45) instead of new factor of Eq. (22). In this case the value of M_{qGT} is found to be 0.708, which is almost same as the value reported in Ref. [30]. Thus we infer that the large value of M_{qGT}-type NMEs is coming through the revisited nucleon currents of Ref. [14] which includes the higher-order term (pseudoscalar term) of the nucleon currents.

C. Neutrino momentum (q) and radial (r) distribution of NME

Further, we have examined the neutrino momentum transfer (q) distribution of NMEs. One can define q-dependent distribution $(C_\alpha(q))$ such that NME defined in Eq. (13) can be written as [36]

$$M_\alpha = \int_0^\infty C_\alpha(q)dq. \tag{46}$$

Distribution of different $C_\alpha(q)$ is shown in Fig. 4. Here NMEs are calculated using the closure method for AV18-type SRC parametrization.

It is found that most of the contributions of NME come from q below 500 MeV. For $C_\nu(q)$-, $C_{\nu\omega}(q)$-, and $C_{2-}(q)$-type NMEs distribution, most contributions come from q around 10 and 160 MeV with a peak value around 0.003 MeV^{-1}. For $C_{1+}(q)$-type distribution, the dominant contribution comes from q of around 350 MeV with a peak value around 0.020 MeV^{-1}, which is significantly larger than the peak value of $C_\nu(q)$- and $C_{\nu\omega}(q)$-type distribution.

Radial distribution of NME is also explored. One can write radial-dependent NME distribution $[C_\alpha(r)]$ [33,36,37] such that

$$M_\alpha = \int_0^\infty C_\alpha(r)dr. \tag{47}$$

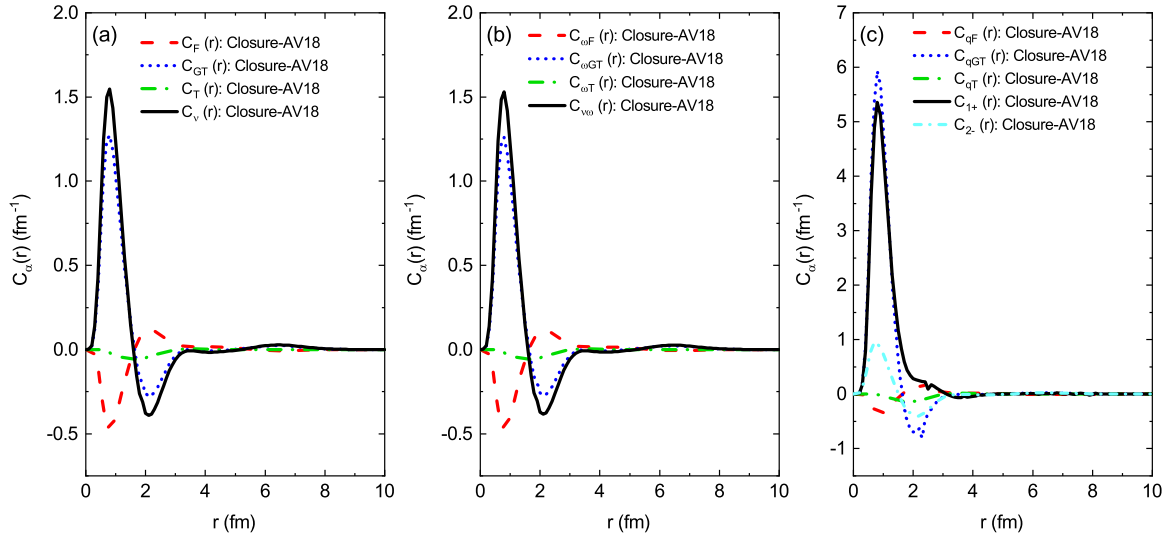

FIG. 5. Radial distribution of NMEs $[C_\alpha(r)]$ with internucleon distance (r). All the NMEs are calculated in the closure method for the AV18 SRC parametrization with closure energy $\langle E\rangle = 0.5$ MeV using the GXPF1A interaction.

Distribution of different $C_\alpha(r)$ is shown in Fig. 5. Here NMEs are calculated using the closure method for AV18-type SRC parametrization with $\langle E\rangle = 0.5$ MeV.

It is found that most of the contribution comes from r less than 4 fm. The $C_\alpha(r)$ peaks around 1 fm with a maximum value of $C_\nu(r)$, and $C_{\nu\omega}(r)$ being near 1.5 fm^{-1}, whereas for $C_{1+}(r)$- and $C_{2-}(r)$-type distributions, maximum values are around 5.5 fm^{-1} and 1 fm^{-1}, respectively.

D. Dependence of NME on spin-parity (J_k^π) of ^{48}Sc

To examine the contribution of each allowed spin-parity (J_k^π) of virtual intermediate states of ^{48}Sc, using Eq. (39) one can write NMEs as function of J_k^π in the running closure method as

$$\mathcal{M}_\alpha(E_c, J_k) = \sum_{J,E_k^*\leqslant E_c} \mathcal{M}_\alpha(J_k, J, E_k^*), \tag{48}$$

and, using Eq. (42), one can write in the running nonclosure method,

$$M_\alpha(E_c, J_k) = \sum_{J,E_k^*\leqslant E_c} M_\alpha(J_k, J, E_k^*). \tag{49}$$

Dependence of Fermi, Gamow-Teller, and tensor NMEs with different J_k^π of ^{48}Sc are shown in Fig. 6. Here NMEs are calculated in the running closure and running nonclosure methods with GXPF1A effective interaction for AV18 SRC parametrization. It is found that for all Fermi-type NMEs,

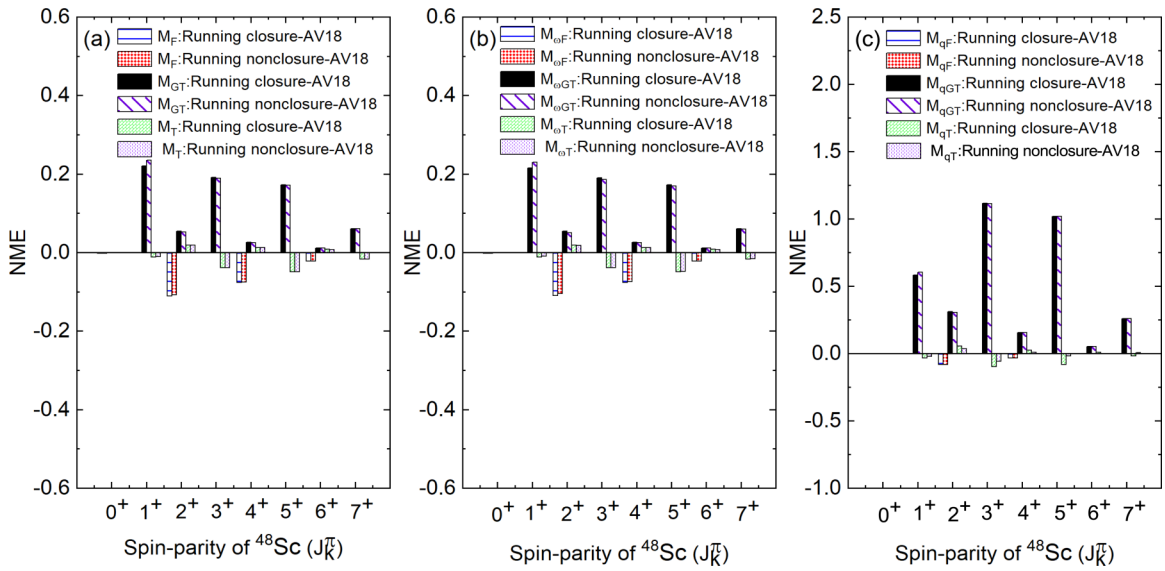

FIG. 6. Contribution through different spin-parity of virtual intermediate states of ^{48}Sc (J_k^π) in NMEs for $m_{\beta\beta}$ and λ mechanisms of $0\nu\beta\beta$ of ^{48}Ca. Here a comparison is shown for NMEs, calculated in the running closure and running nonclosure methods with GXPF1A effective interaction for AV18 SRC parametrization. $\langle E\rangle = 0.5$ MeV is used for the running closure method.

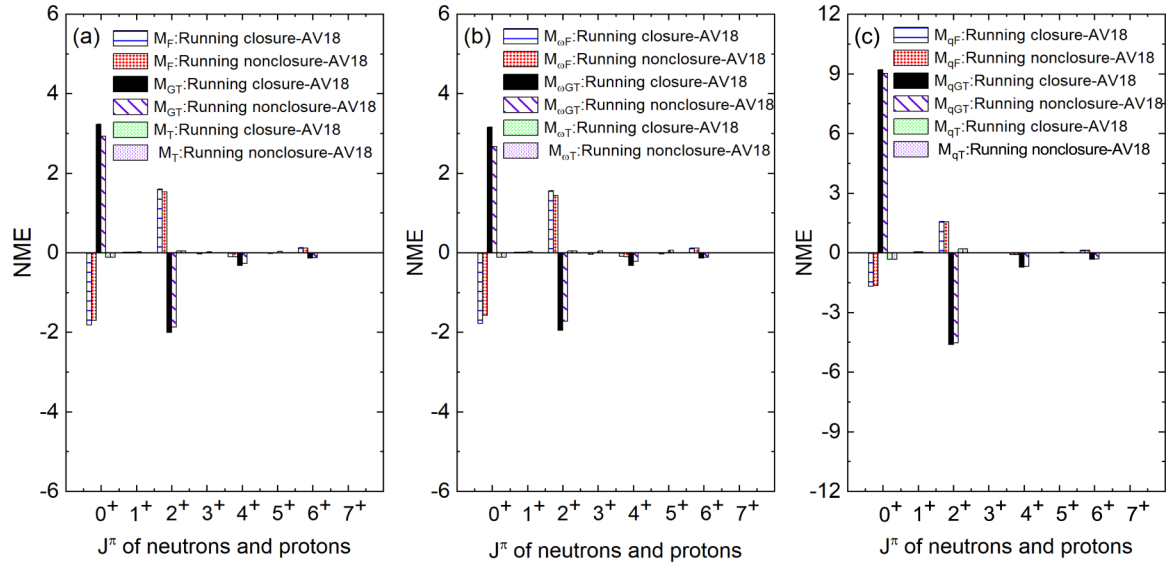

FIG. 7. Contribution through different coupled spin-parity of two initial neutrons or two final created protons (J^π) in NMEs for $m_{\beta\beta}$ and λ mechanisms of $0\nu\beta\beta$ of ^{48}Ca. Here a comparison is shown for NMEs calculated in the running closure and running nonclosure methods with GXPF1A effective interaction for AV18 SRC parametrization. $\langle E\rangle = 0.5$ MeV is used for the running closure method.

contribution through each J^π_k is negative, and for Gamow-Teller all contribution is positive. Contribution in tensor NMEs comes in the opposite phase for different J^π_k, reducing the total tensor NMEs. Further, it is found that the dominant contribution comes from the 2^+ state for M_F- and $M_{\omega F}$-type NMEs and with a small contribution from the 4^+ and 6^+ states. Contributions through the 0^+ and odd-J^π_k states are negligible. For M_{qF}-type NMEs, the dominant contribution comes from the 2^+ and 4^+ states. For all Fermi-type NMEs, enhancements in the running nonclosure method are very small as compared to the running closure method.

For M_{GT}-, $M_{\omega GT}$-, and M_{qGT}-type NMEs, all J^π_k contributes significantly except 0^+. Dominating contribution come through 1^+, 3^+, and 5^+ states for M_{GT}- and $M_{\omega GT}$-type NMEs, whereas for M_{qGT}-type NMEs, the order of most dominant contributions are from the 3^+, 5^+, and 1^+ states. Small enhancement in NMEs with the running nonclosure method is found from 1^+ states as compared to NMEs in the running closure method.

For M_T- and $M_{\omega T}$-type NMEs, all negative contributions come from 1^+, 3^+, 5^+, and 7^+ states with contributions from the 3^+ and 5^+ states being dominant. Contributions through 2^+, 4^+, and 6^+ are all positive. For M_{qT}-type NMEs, the bulk of the negative contributions comes from the 3^+ state with additional negative contributions from the 1^+ and 5^+ states. The dominating positive contribution from 2^+ states with a very small positive contribution from the 4^+ state. A similar pattern of variation of the different types of NMEs with J^π_k are seen with other types of SRC parametrizations.

E. Dependence of NME on coupled spin-parity (J^π) of two decaying neutrons and two created protons

We have also checked the variation of NMEs with coupled spin-parity (J^π) of two decaying neutrons and two created protons in the decay. One can write using Eqs. (39) and (42) NMEs as function of J^π in the running closure method as

$$\mathcal{M}_\alpha(E_c, J) = \sum_{J_k, E^*_k \leqslant E_c} \mathcal{M}_\alpha(J_k, J, E^*_k) \tag{50}$$

and in the running nonclosure method as

$$M_\alpha(E_c, J) = \sum_{J_k, E^*_k \leqslant E_c} M_\alpha(J_k, J, E^*_k). \tag{51}$$

Contributions of NMEs through different J^π is shown in Fig. 7. Here NMEs are calculated in the running closure and running nonclosure methods for AV18 SRC parmaetrization.

For all types of NMEs, the most dominant contribution comes from 0^+ states and 2^+ states. Also, the contribution from the 0^+ and 2^+ states is of opposite sign, reducing the total NMEs. The small contribution comes from the 4^+ and 6^+ states with almost negligible contributions from odd-J^π states. A pairing effect is responsible for the dominant even-J^π contributions [19].

F. Variation of NME for $0\nu\beta\beta$ with the cutoff excitation energy (E_c) and the cutoff number of states (N_c) of ^{48}Sc

Dependence of NMEs with cutoff excitation energy (E_c) of the intermediate nucleus ^{48}Sc is examined. One can write, using Eq. (39), NMEs as the function E_c in the running closure method as

$$\mathcal{M}_\alpha(E_c) = \sum_{J_k, J, E^*_k \leqslant E_c} \mathcal{M}_\alpha(J_k, J, E^*_k) \tag{52}$$

and, using Eq. (42), NMEs in the running nonclosure method as

$$M_\alpha(E_c) = \sum_{J_k, J, E^*_k \leqslant E_c} M_\alpha(J_k, J, E^*_k). \tag{53}$$

Variation of the Fermi, Gamow-Teller, tensor, and total NMEs with cutoff excitation energy (E_c) of ^{48}Sc is shown in Fig. 8.

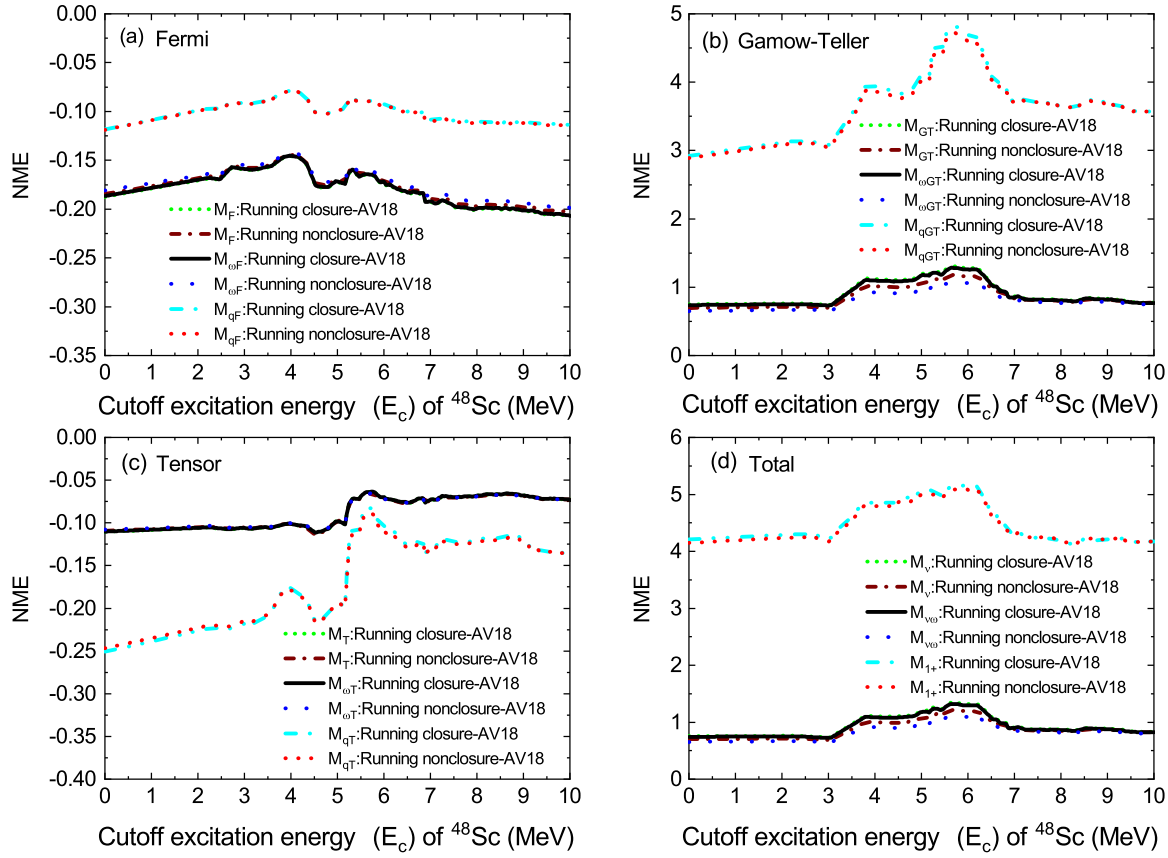

FIG. 8. Variation of (a) Fermi, (b) Gamow-Teller, (c) tensor, and (d) total NMEs for $0\nu\beta\beta$ ($m_{\beta\beta}$ and λ mechanisms) of ^{48}Ca with cutoff excitation energy (E_c) of states of virtual intermediate nucleus ^{48}Sc. NMEs are calculated with total GXPF1A interaction for AV18 SRC parametrization in the running closure and running nonclosure methods. For the running closure method, closure energy $\langle E\rangle = 0.5$ MeV is used.

Here we have shown the dependence of NMEs for $E_c = 0$ to 10 MeV. The NMEs are calculated in the running closure and running nonclosure methods for AV18-type SRC parametrization. It is observed that the first few low-lying states for each J_k^π mostly contribute constructively and destructively. After about $E_c = 7$ MeV, NMEs attain mostly stable values. At large-enough values of E_c, NMEs becomes constant. A similar variation of NMEs with E_c are found for other SRC parametrizations for different types of NMEs.

It is also possible to set a cutoff on the number of states (N_c) for each allowed J_k^π of ^{48}Sc to calculate the NMEs. One can write the NMEs as function of the cutoff number of states (N_c) of ^{48}Sc in the running closure method as

$$\mathcal{M}_\alpha^{0\nu}(N_c) = \sum_{J_k, J, N_k \leqslant N_c} \mathcal{M}_\alpha^{0\nu}(J_k, J, N_k), \tag{54}$$

and in running nonclosure method as

$$M_\alpha(N_c) = \sum_{J_k, J, N_k \leqslant N_c} M_\alpha(J_k, J, N_k), \tag{55}$$

where $\mathcal{M}_\alpha(J_k, J, N_k)$ and $M_\alpha(J_k, J, N_k)$ is same as Eqs. (39) and (42), respectively. The dependence of different Fermi, Gamow-Teller, tensor, and total NMEs with N_c is shown in Fig. 9. Here NMEs are calculated with total GXPF1A interaction in the running closure and running nonclosure methods for AV18 SRC parametrization. The dependence shows that the first few low-lying states mostly contribute constructively and destructively. After $N_c = 75$, different types of NMEs attain a stable value. At a large value of N_c, NMEs becomes mostly constant. In our calculation, we have considered $N_c = 150$ for each allowed J_k^π of ^{48}Sc, which gives NMEs with negligible uncertainty. A similar dependence of NMEs with N_c are seen for other SRC parametrizations.

G. Variation of NME for $2\nu\beta\beta$ with E_c and N_c of ^{48}Sc

To complete the discussion on the dependence of NME on E_c and N_c, we have also examined the NME versus E_c and N_c for two-neutrino double beta decay ($2\nu\beta\beta$), which is similar to $0\nu\beta\beta$, except $2\nu\beta\beta$ is a lepton number-conserving decay, where two antineutrinos come into the final state along with two electrons. The $2\nu\beta\beta$ process for ^{48}Ca is written as

$$^{48}\mathrm{Ca} \rightarrow {}^{48}\mathrm{Ti} + e^- + e^- + \overline{\nu}_e + \overline{\nu}_e. \tag{56}$$

The half-life of $2\nu\beta\beta$ of the 0^+ ground state (g.s.)–to–0^+ ground state transition is given by [38]

$$T_{1/2}^{2\nu,0} = F_0^{2\nu} \left| M_{GT}^{2\nu}(0^+) \right|^2, \tag{57}$$

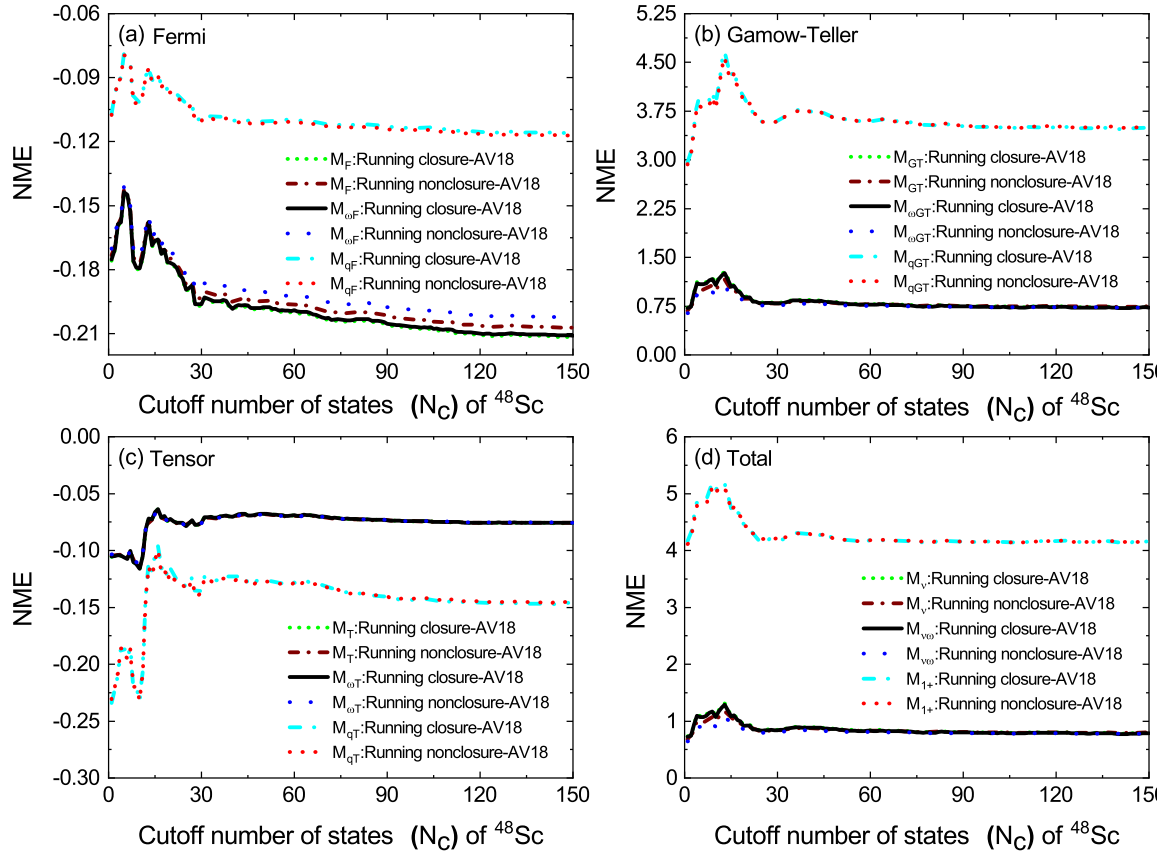

FIG. 9. Variation of (a) Fermi, (b) Gamow-Teller, (c) tensor, and (d) total NMEs for $0\nu\beta\beta$ ($m_{\beta\beta}$ and λ mechanisms) of ^{48}Ca with cutoff number of states (N_c) of virtual intermediate nucleus ^{48}Sc. NMEs are calculated with total GXPF1A interaction for AV18 SRC parametrization in the running closure and running nonclosure methods. For the running closure method, closure energy $\langle E\rangle = 0.5$ MeV is used.

where $F_0^{2\nu}$ is the phase-space factor [38]. Here only Gamow-Teller-type NMEs $[M_{GT}^{2\nu}(0^+)]$ are relevant, which can be written as [38]

$$M_{GT}^{2\nu}(0^+) = \sum_{k,E_k^*\leqslant E_c} \frac{\langle f||\sigma\tau^-||k\rangle\langle k||\sigma\tau^-||i\rangle}{E_k^* + E_0}, \qquad (58)$$

where τ^- is the isospin-lowering operator; in the present work $|i\rangle$ is 0^+ ground state of the parent nucleus ^{48}Ca, $|f\rangle$ is 0^+ ground state of the granddaughter nucleus ^{48}Ti, $|k\rangle$ is the 1^+ states of intermediate nucleus ^{48}Sc, E_k^* is the excitation energy of the 1^+ states of ^{48}Sc, and the constant E_0 is given by

$$E_0 = \tfrac{1}{2}Q_{\beta\beta}(0^+) + \triangle M. \qquad (59)$$

Here $Q_{\beta\beta}(0^+)$ is the Q value corresponding to $\beta\beta$ decay of ^{48}Ca and $\triangle M$ is mass difference of ^{48}Sc and ^{48}Ca isotopes.

The dependence of NMEs for $2\nu\beta\beta$ on E_c of the 1^+ states of virtual intermediate nucleus ^{48}Sc is shown in Fig. 10. It is found that the first few low-lying states up to around 7 MeV contribute constructively and destructively. The NMEs are mostly saturated and become constant at high excitation energy.

Variations of NME for $2\nu\beta\beta$ with the N_c of virtual intermediate nucleus ^{48}Sc are given in Fig. 11. Here NME is calculated with total GXPF1A interaction. It is observed that the first 50 low-lying states contribute constructively and destructively. At a large N_c, NME becomes constant.

It is important to mention that the dependence of NME with J_k^π, and J^π for the light neutrino-exchange ($m_{\beta\beta}$) mechanism of $0\nu\beta\beta$ of ^{48}Ca is also presented in Figs. 3

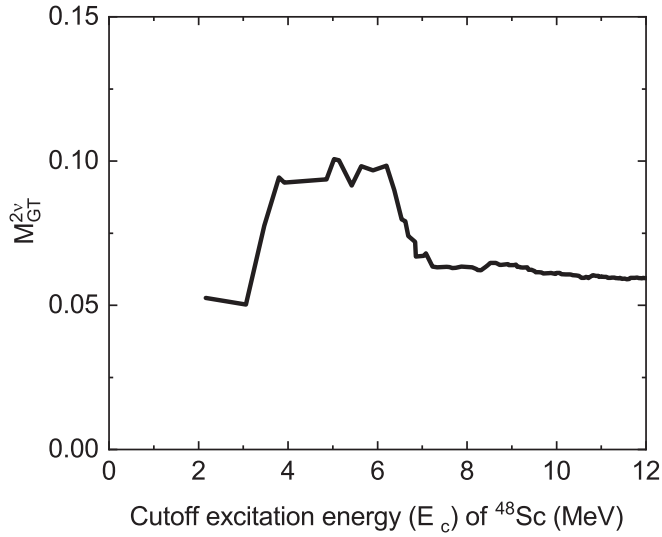

FIG. 10. Variation of NME for $2\nu\beta\beta$ of ^{48}Ca with cutoff excitation energy (E_c) of 1^+ states of the virtual intermediate nucleus ^{48}Sc.

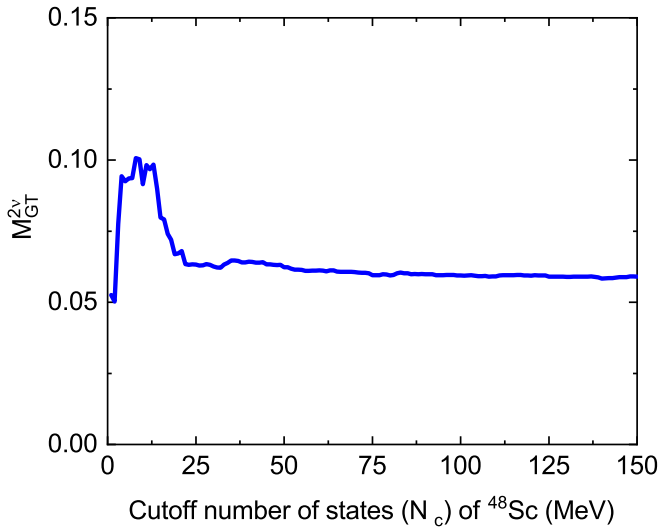

FIG. 11. Variation of NME for $2\nu\beta\beta$ of ^{48}Ca with cutoff number of 1^+ states (N_c) of the virtual intermediate nucleus ^{48}Sc.

and 4, respectively, of Ref. [18] using the running closure and nonclosure methods. Also, the variation of NMEs with number of intermediate states are explored for the fictitious $0\nu\beta\beta$ of ^{44}Ca, and ^{46}Ca. Further, the convergence of total NME with excitation energy of intermediate states for $0\nu\beta\beta$ of ^{48}Ca is examined in Fig. 5 of Ref. [18]. The motivations and some of the figures presented in the current study for the $m_{\beta\beta}$ mechanism of $0\nu\beta\beta$ of ^{48}Ca are similar to those in Ref. [18].

V. SUMMARY AND CONCLUSIONS

Different types of NMEs for $m_{\beta\beta}$ and λ mechanisms of $0\nu\beta\beta$, which have their origin in the left-right symmetric model with right-handed gauge boson at TeV scale, are calculated in ISM for one of the $0\nu\beta\beta$ decay candidates, ^{48}Ca. The GXPF1A effective interaction of the pf shell is used to calculate NMEs in both the closure and nonclosure approaches. The standard effects of FNS and the revisited higher-order terms, such as the pseudoscalar and weak magnetism terms of nucleon currents, which are exploited in Refs. [14,29], are also included the present work. The short-range nature of nucleon-nucleon interactions is also taken care of in Miller-Spencer, CD-Bonn, and AV18 SRC parametrizations. Detailed comparative results are presented for closure versus nonclosure approaches using four different methods: closure, running closure, running nonclosure, and mixed methods. The significant enhancements of M_{qGT}- and M_{qT}-type NMEs are found for the inclusion of the new pseudoscalar term of nucleon currents.

We have extracted the optimal values of $\langle E\rangle$, which are 0.20, 0.65, 0.30, and 0.67 MeV, for M_ν-, $M_{\nu\omega}$-, M_{1+}-, and M_{2-}-type NMEs, respectively. At optimal $\langle E\rangle$, NMEs in the closure and mixed methods have the same value. Also, we found that there is a less than 1% change in NMEs when using $\langle E\rangle = 0.5$ MeV instead of optimal $\langle E\rangle$. Thus, we have used $\langle E\rangle = 0.5$ MeV for calculating NME for $0\nu\beta\beta$ of ^{48}Ca with the GXPF1A interaction to compare the different types of NMEs consistently.

Results show that NMEs in the closure and nonclosure approaches are very similar if we use $\langle E\rangle = 0.5$ MeV, which is close to the optimal value of closure energy. The M_{qGT}-type NME is found to be much larger than the M_{GT}- and $M_{\omega GT}$-type NMEs, which is shown for the inclusion pseudoscalar term of the nucleon currents for M_{qGT} NMEs.

Variations of NMEs in the running closure and mixed methods with closure energy $\langle E\rangle$ are also studied. For changing $\langle E\rangle = 0$ to 10 MeV, there is about a 11% decrement of M_ν-type NMEs in the running closure method. In this case, $M_{\nu\omega}$-type NMEs decrease by about 19% and M_{1+}-type NME decrease by about 2.5% in the running closure method. In all these cases, there are negligible changes in NMEs in the mixed method.

The distributions of NMEs with neutrino momentum transfer $[C_\alpha(q)]$ and internucleon distance$(C_\alpha(r))$ are examined. For $C_\nu(q)$-, $C_{\nu\omega}(q)$-, and $C_{2-}(q)$-type NME distributions, most of the contributions comes from q around 10 and 160 MeV with a peak value around 0.003 MeV^{-1}. For $C_{1+}(q)$-type distributions, the dominant contribution comes from q around 350 MeV with a peak value around 0.020 MeV^{-1}, which is significantly larger than the peak value of $C_\nu(q)$- and $C_{\nu\omega}(q)$-type NMEs. The radial distribution $C_\alpha(r)$ peak around 1 fm with maximum value of $C_\nu(r)$ and $C_{\nu\omega}(r)$ is near 1.5 fm^{-1}, whereas for $C_{1+}(r)$- and $C_{2-}(r)$-type distributions, maximum values are around 5.5 and 1 fm^{-1}, respectively.

We have examined the contribution of each spin-parity (J^π_k) of the intermediate nucleus ^{48}Sc in NMEs running closure and running nonclosure methods. It is observed that 2^+ and 4^+ states have dominant contributions in M_F-, $M_{\omega F}$-, and M_{qF}-type NMEs. For M_{GT}, $M_{\omega GT}$, and M_{qGT}-type NMEs, the 1^+, 3^+, and 5^+ states contribute the most. Contributions of all J^π_k are negative for the Fermi-type NMEs and positive for the Gamow-Teller-type NMEs. For M_T, $M_{\omega T}$-type NMEs, all contributions are negative for the 1^+, 3^+, 5^+, and 7^+ states and positive for the 2^+, 4^+, and 6^+ states. For M_{qT}-type NMEs, the dominant negative contribution comes from the 3^+state and the positive contribution comes from the 2^+ state.

We have also checked the dependence of the NMEs calculated in the running nonclosure and running closure methods with coupled spin-parity of two initial neutrons or final created protons (J^π) of the decay. It is found that the dominant contribution comes from the 0^+ and 2^+ states with their phases being opposite, which reduces the total NMEs.

Dependence of different types of NMEs with cutoff excitation energy (E_c) and the cutoff number of states (N_c) of the intermediate nucleus (^{48}Sc) are also explored. It is found that only the first few low-lying states contribute constructively and destructively in NMEs, and at large N_c and E_c, NMEs become almost constant. In our case, we have considered $N_c = 150$ for each J^π_k of ^{48}Sc with uncertainty being very small. Similar types of dependence are found for $2\nu\beta\beta$ NMEs.

ACKNOWLEDGMENTS

S.S. thanks the Ministry of Human Resource Development (MHRD), Government of India, for the financial assistance toward Ph.D. work. Y.I. acknowledges the support from JSPS KAKENHI Grant No.17K05440.

[1] J. Schechter and J. W. F. Valle, Neutrinoless double-β decay in SU (2)× U (1) theories, Phys. Rev. D **25**, 2951 (1982).

[2] F. F. Deppisch, M. Hirsch, and H. Päs, Neutrinoless double-beta decay and physics beyond the standard model, J. Phys. G: Nucl. Part. Phys. **39**, 124007 (2012).

[3] W. Rodejohann, Neutrino-less double beta decay and particle physics, Int. J. Mod. Phys. E **20**, 1833 (2011).

[4] M. Aker *et al.* (KATRIN Collaboration), Improved Upper Limit on the Neutrino Mass from a Direct Kinematic Method by Katrin, Phys. Rev. Lett. **123**, 221802 (2019).

[5] T. Tomoda, Double beta decay, Rep. Prog. Phys. **54**, 53 (1991).

[6] F. T. Avignone, S. R. Elliott, and J. Engel, Double beta decay, majorana neutrinos, and neutrino mass, Rev. Mod. Phys. **80**, 481 (2008).

[7] V. Rodin, A. Faessler, F. Šimkovic, and P. Vogel, Assessment of uncertainties in QRPA $0\nu\beta\beta$-decay nuclear matrix elements, Nucl. Phys. A **766**, 107 (2006).

[8] F. Šimkovic, G. Pantis, J. D. Vergados, and A. Faessler, Additional nucleon current contributions to neutrinoless double β decay, Phys. Rev. C **60**, 055502 (1999).

[9] J. D. Vergados, H. Ejiri, and F. Šimkovic, Theory of neutrinoless double-beta decay, Rep. Prog. Phys. **75**, 106301 (2012).

[10] R. N. Mohapatra and G. Senjanović, Neutrino Mass and Spontaneous Parity Nonconservation, Phys. Rev. Lett. **44**, 912 (1980).

[11] R. N. Mohapatra and J. D. Vergados, New Contribution to Neutrinoless Double Beta Decay in Gauge Models, Phys. Rev. Lett. **47**, 1713 (1981).

[12] R. N. Mohapatra, New contributions to neutrinoless double-beta decay in supersymmetric theories, Phys. Rev. D **34**, 3457 (1986).

[13] J. Vergados, Neutrinoless double β-decay without Majorana neutrinos in supersymmetric theories, Phys. Lett. B **184**, 55 (1987).

[14] F. Šimkovic, D. Štefánik, and R. Dvornický, The λ mechanism of the $0\nu\beta\beta$-decay, Front. Phys. **5**, 57 (2017).

[15] J. Engel and J. Menéndez, Status and future of nuclear matrix elements for neutrinoless double-beta decay: A review, Rep. Prog. Phys. **80**, 046301 (2017).

[16] E. Caurier, J. Menéndez, F. Nowacki, and A. Poves, Influence of Pairing on the Nuclear Matrix Elements of the Neutrinoless $\beta\beta$ Decays, Phys. Rev. Lett. **100**, 052503 (2008).

[17] M. Horoi and S. Stoica, Shell model analysis of the neutrinoless double-β decay of ^{48}Ca, Phys. Rev. C **81**, 024321 (2010).

[18] R. A. Sen'kov and M. Horoi, Neutrinoless double-β decay of ^{48}Ca in the shell model: Closure versus nonclosure approximation, Phys. Rev. C **88**, 064312 (2013).

[19] B. A. Brown, M. Horoi, and R. A. Sen'kov, Nuclear Structure Aspects of Neutrinoless Double-β Decay, Phys. Rev. Lett. **113**, 262501 (2014).

[20] Y. Iwata, N. Shimizu, T. Otsuka, Y. Utsuno, J. Menéndez, M. Honma, and T. Abe, Large-Scale Shell-Model Analysis of the Neutrinoless $\beta\beta$ Decay of ^{48}Ca, Phys. Rev. Lett. **116**, 112502 (2016).

[21] J. Barea and F. Iachello, Neutrinoless double-β decay in the microscopic interacting boson model, Phys. Rev. C **79**, 044301 (2009).

[22] J. Barea, J. Kotila, and F. Iachello, Limits on Neutrino Masses from Neutrinoless Double-β Decay, Phys. Rev. Lett. **109**, 042501 (2012).

[23] T. R. Rodríguez and G. Martínez-Pinedo, Energy Density Functional Study of Nuclear Matrix Elements for Neutrinoless $\beta\beta$ Decay, Phys. Rev. Lett. **105**, 252503 (2010).

[24] L. S. Song, J. M. Yao, P. Ring, and J. Meng, Relativistic description of nuclear matrix elements in neutrinoless double-β decay, Phys. Rev. C **90**, 054309 (2014).

[25] P. K. Rath, R. Chandra, K. Chaturvedi, P. K. Raina, and J. G. Hirsch, Uncertainties in nuclear transition matrix elements for neutrinoless $\beta\beta$ decay within the projected-Hartree-Fock-Bogoliubov model, Phys. Rev. C **82**, 064310 (2010).

[26] S. Pastore, J. Carlson, V. Cirigliano, W. Dekens, E. Mereghetti, and R. B. Wiringa, Neutrinoless double-β decay matrix elements in light nuclei, Phys. Rev. C **97**, 014606 (2018).

[27] X. B. Wang, A. Hayes, J. Carlson, G. Dong, E. Mereghetti, S. Pastore, and R. B. Wiringa, Comparison between variational Monte Carlo and shell model calculations of neutrinoless double beta decay matrix elements in light nuclei, Phys. Lett. B **798**, 134974 (2019).

[28] V. Cirigliano, W. Dekens, J. de Vries, M. L. Graesser, E. Mereghetti, S. Pastore, M. Piarulli, U. van Kolck, and R. B. Wiringa, Renormalized approach to neutrinoless double-β decay, Phys. Rev. C **100**, 055504 (2019).

[29] D. Štefánik, R. Dvornický, F. Šimkovic, and P. Vogel, Reexamining the light neutrino exchange mechanism of the $0\nu\beta\beta$ decay with left- and right-handed leptonic and hadronic currents, Phys. Rev. C **92**, 055502 (2015).

[30] M. Horoi and A. Neacsu, Shell model study of using an effective field theory for disentangling several contributions to neutrinoless double-β decay, Phys. Rev. C **98**, 035502 (2018).

[31] S. Sarkar, P. Kumar, K. Jha, and P. K. Raina, Sensitivity of nuclear matrix elements of $0\nu\beta\beta$ of ^{48}Ca to different components of the two-nucleon interaction, Phys. Rev. C **101**, 014307 (2020).

[32] F. Šimkovic, A. Faessler, H. Müther, V. Rodin, and M. Stauf, $0\nu\beta\beta$-decay nuclear matrix elements with self-consistent short-range correlations, Phys. Rev. C **79**, 055501 (2009).

[33] F. Šimkovic, A. Faessler, V. Rodin, P. Vogel, and J. Engel, Anatomy of the $0\nu\beta\beta$ nuclear matrix elements, Phys. Rev. C **77**, 045503 (2008).

[34] B. Brown and W. Rae, The shell-model code NuShellX@MSU, Nucl. Data Sheets **120**, 115 (2014).

[35] R. A. Sen'kov and M. Horoi, Accurate shell-model nuclear matrix elements for neutrinoless double-β decay, Phys. Rev. C **90**, 051301(R) (2014).

[36] J. Menéndez, Neutrinoless $\beta\beta$ decay mediated by the exchange of light and heavy neutrinos: The role of nuclear structure correlations, J. Phys. G: Nucl. Part. Phys. **45**, 014003 (2017).

[37] J. Menéndez, A. Poves, E. Caurier, and F. Nowacki, Disassembling the nuclear matrix elements of the neutrinoless $\beta\beta$ decay, Nucl. Phys. **818**, 139 (2009).

[38] M. Horoi, S. Stoica, and B. A. Brown, Shell-model calculations of two-neutrino double-β decay rates of ^{48}Ca with the GXPF1A interaction, Phys. Rev. C **75**, 034303 (2007).